J. Water Environ. Nanotechnol., 7(1): 14-30 Winter 2022

ORIGINAL RESEARCH PAPER

Removal of Cefixime Using Heterogeneous Fenton Catalysts: Alginate/Magnetite Hydroxyapatite Nanocomposite

Mona Nabizad, Ahmad Dadvand Koohi*, Zahra Erfanipour

Chemical Engineering Department, Engineering Faculty, University of Guilan, Rasht, Iran

Received: 2021-12-08 Accepted: 2022-01-25 Published: 2022-02-01

ABSTRACT

In this study, alginate, magnetite, and hydroxyapatite were used to fabricate alginate-hydroxyapatite (Alg-Hap), alginate-Fe_3O_4 (Alg-Fe_3O_4), and alginate-magnetic hydroxyapatite (Alg-mHap) using ferric chloride (III) crosslinker to remove cefixime from an aqueous solution. FTIR, SEM, VSM, BET, and XRD tests were used to determine the functional groups, morphology, magnetization behavior, surface area, and crystallinity of catalysts, respectively. The optimal pH for the Fenton reaction was determined to be 3.3 for Alg-Hap and Alg-Fe_3O_4 catalysts and 4 for Alg-mHap catalysts. Increases in the concentration of hydrogen peroxide (1 to 3 mM) and the amount of catalyst (50 to 90 gr/L) increased the percentage of degradation to approximately 8% and 6%, respectively. The degradation efficiency of cefixime by using Alg-mHap as the best catalyst in the Fenton process was achieved 91%, at optimum condition (pH of 4, catalyst amount of 90 gr/L, initial cefixime concentration of 5 mg/L, H_2O_2 concentration of 3 mM within 90 min). Moreover, the second-order kinetic equation fits the experimental data for cefixime degradation for all three catalysts. Furthermore, not only did the catalysts display a negligible iron leaching (0.92 mg/L for Alg-mHap) but also after three consecutive cycles, the catalysts indicated long-term stability. Comparison between synthesized catalysts and other methods proved its effectiveness.

Keywords: *Alginate, Heterogeneous Catalysts, Fenton, Degradation, Mechanism*

How to cite this article

Nabizad M., Dadvand Koohi A., Erfanipour Z. Removal of Cefixime Using Heterogeneous Fenton Catalysts: Alginate/Magnetite Hydroxyapatite Nanocomposite. J. Water Environ. Nanotechnol., 2022; 7(1): 14-30.

DOI: 10.22090/jwent.2022.01.002

INTRODUCTION

In recent years, numerous pharmaceutical wastes have been detected in wastewater, groundwater, surface water, and drinking water. Given that drug compounds can cause widespread changes in the ecosystem, their persistence in the aquatic environment is a cause for concern. Antibiotics are one of the most severe pharmaceutical concerns [1]. Antibiotics are chemical compounds that inhibit the growth of microorganisms; however, they are frequently derived from microorganisms and are synthesized semi-artificially or artificially [2–4]. Antibiotics have a variety of uses, including treatment of microbial infection and as feed additives. However, because their metabolism is incomplete, most of it is returned to the environment, where their excessive spread causes complications such as aquatic environment toxicity and increased resistance to pathogenic bacteria. Additionally, these compounds can persist in the environment for an extended time [5]. Approximately 40% to 50% of antibiotics are excreted in the urine and are subsequently released into the environment via hospital and domestic sewage. Due to limited water resources and the dangers of antibiotics, it is deemed critical to remove these contaminants [6]. Cefixime is one of these antibiotics; it is a third-generation cephalosporin with the molecular

* Corresponding Author Email: *dadvand@guilan.ac.ir*

formula $C_{16}H_{15}N_5O_7S_2$ and a molecular weight of 453 g/mole. Cefixime is chemically unstable, and its solubility in water is pH-dependent. It is used to treat bacterial infections such as pneumonia, bronchitis, syphilis, and infections of the ear, throat, lung, and urinary tract [7,8].

Antibiotics can be eliminated physically, chemically, or biologically. Filtration, coagulation, ion exchange, membrane separation, and adsorption are all physical methods [9,10]. It is important to note that these methods do not eliminate the pollutant but rather transfer it from one phase to another. Chemical methods include the advanced oxidation process (AOP), which is one of the most well-known, ozone, ultrasonic, photochemical, electro Fenton, photo Fenton, and Fenton reactions, the latter of which is one of the most well-known the most attractive [1,11,12]. The advantages of this method include its high degradation efficiency, simplicity (it can be performed at room temperature and pressure), and ability to purify a wide variety of contaminants. It is also non-toxic, cost-effective, and stable. The Fenton reaction is catalyzed by hydrogen peroxide and aqueous ferrous irons, resulting in the formation of hydroxyl free radicals, which are highly reactive with organic compounds (Equation 1) [13–15]:

$$Fe^{2+} + H_2O_2 \rightarrow OH^{\bullet} + Fe^{3+} + OH^{-} \quad (1)$$

The reaction of Fe^{3+} with H_2O_2 (Fenton-like reaction) proceeds through the generation of hydroperoxyl radical ($HO_2^{\bullet}$) as follows:

$$Fe^{3+} + H_2O_2 \rightarrow Fe^{2+} + HO_2^{\bullet} + H^{+} \quad (2)$$

$$Fe^{3+} + HO_2^{\bullet} \rightarrow Fe^{2+} + H^{+} + O_2 \quad (3)$$

$$Fe^{2+} + OH^{\bullet} \rightarrow Fe^{3+} + OH^{-} \quad (4)$$

$$H_2O_2 + OH^{\bullet} \rightarrow HO_2^{\bullet} + H_2O \quad (5)$$

$$Fe^{2+} + HO_2^{\bullet} \rightarrow Fe^{3+} + HO_2^{-} \quad (6)$$

The Fenton and photo-Fenton reactions are sensitive to the amount of H_2O_2 and iron added and the operating pH value [11,16]. The Fenton process is classified into two distinct types: homogeneous and heterogeneous Fenton. The distinction between these two methods is in the location of the catalytic reaction. Catalytic activity occurs throughout the liquid phase in the homogeneous Fenton process, whereas catalytic activity occurs at the catalyst surface in the heterogeneous Fenton process. The Fenton process involves the addition of a homogeneous iron (II) catalyst directly to the medium, which results in the formation of a large ferric sludge that is considered contamination and requires a complex process to remove [17]. Additionally, iron catalysts are generally not recyclable in their homogeneous form and require acidic conditions with a pH less than 3, which is not cost-effective; thus, a catalyst that performs better in acidic conditions should be used to be recovered and reused [18,19].

Due to the high magnetic properties of magnetite (Fe_3O_4) nanoparticles, they are used in various fields, including adsorption of bio pollutants, cancer treatment, and release and drug delivery. Additional characteristics include low toxicity, ease of coverage, and modification [20–22]. Mostafa loo et al. (2019) used magnetic bismuth ferrite nanoparticles to study the photocatalytic degradation of cefixime in an aqueous solution under visible light. Additionally, the best experimental conditions resulted in a maximum degradation rate of up to 91.8% [6].

Furthermore, polymers such as sodium alginate, a cost-effective, non-toxic, and biodegradable natural biopolymer, are used nowadays to preserve and immobilize iron ions and prevent their deposition in solution. Due to its carboxylate groups and anions' adsorption properties, this polymer is used in the adsorption process. Iron nanoparticles are well-dispersed within the alginate polymer network and act as a catalyst substrate [23,24]. Due to antibiotic adsorption, hydroxyapatite is an effective filler in the catalyst structure. Moreover, this nanomaterial is environmentally friendly due to its unique structural properties, biodegradability, and high adsorption. As a result, it is widely used in water treatment [25,26]. Ergüt et al. (2019) investigated the decolorization of malachite green using a heterogeneous Fenton reaction and a nanocomposite of iron oxide and hydroxyapatite. Their findings indicated that the synthesized catalyst was highly efficient in the Fenton reaction, achieving 100% decolorization efficiency after six uses [27]. Hassani et al. (2020) investigated the effect of the sono-electro-Fenton process on the removal of cefixime from water using the RSM method and the microorganism toxicity of the effluent. Following that, the results indicated that

the sono-electro Fenton process effectively removed cefixime to a maximum of 97.5% [1]. The loss of oxidants due to H_2O_2's radical-scavenging effect, the continuous leaching of iron ions and formation of solid sludge, and H_2O_2 self-decomposition are the primary disadvantages of using Fenton reactions in wastewater treatment may affect the process's environmental and economic viability. To circumvent these constraints, loading iron species onto solid or polymer network support appears to be a promising method for generating heterogeneous catalysts.

In this study, first hydroxyapatite was synthesized from fish scales, and then new catalysts were synthesized by loading magnetic and hydroxyapatite NPs into the alginate polymer network, which was ionically crosslinked using a simple protocol. These beads could be beneficial as catalysts in the heterogeneous Fenton process because the numerous functional groups distributed along the Alg chains stabilize iron ions without using chelating agents or organic solvents. Additionally, MNPs can act as Fenton catalysts, and trapping Fe_3O_4 nanoparticles within the alginate polymer network facilitates their removal from the solution. Moreover, Hap as catalyst support strengthens the catalyst beads and possesses excellent adsorption properties, resulting in pollutant adsorption on the catalyst surface and subsequent degradation by the oxidizing species produced. Apart from that, these solid catalysts may reduce iron ion loss, thereby preventing the formation of solid sludge and secondary contamination of treated water. Therefore, if Alg, Hap, and Fe_3O_4 are rationally integrated into a ternary composite, there would be synergistic effects for the enhancement of Fenton performance. To the best of our knowledge, this is the first study on the heterogeneous Fenton degradation of cefixime using Alg modified by Hap and Fe_3O_4 NPs. Herein, (1) the feasibility of alginate-magnetite (Alg-Fe_3O_4), alginate-hydroxyapatite (Alg-Hap), and alginate-magnetic hydroxyapatite (Alg-mHap) as heterogeneous Fenton catalysts in the degradation of cefixime, a representative antibiotic widely used, was investigated. (2) It would be expected that the performance of Alg-mHap ternary composite would surpass those of binary Alg-Fe_3O_4 and Alg-Hap in the Fenton process. First, the structure and morphology of synthesized catalysts were specified using Fourier transform infrared spectroscopy (FTIR), X-ray diffraction, Brunauer-Emmett-Teller (BET), vibrating sample magnetometer (VSM), and field emission scanning electron microscopy (FESEM). Then, all-controlling factors which are cefixime and hydrogen peroxide concentrations in the aqueous medium, and changes in catalyst concentration and initial pH were evaluated, as well as the mechanisms underlying the highly efficient Fenton activity. The rapid separation and efficient recycling of catalysts after the Fenton process was considered.

MATERIALS AND METHODS

Materials

Scales of Rutilus kutum were obtained from the bazaar of Bandar Anzali (Iran). Cefixime was obtained from Pars Daroo Company in Iran, whereas sodium alginate ($C_6H_7O_6Na$) and ammonium hydroxide (25%) were obtained from Sigma Aldrich and Merck, respectively. $FeSO_4.7H_2O$ and $FeCl_3.6H_2O$ were obtained from the Qatran Shimi Company (Iran) to prepare Fe_3O_4 nanoparticles.

Synthesis of hydroxyapatite nanoparticles

The synthesis of hydroxyapatite from fish scales was carried out following Kongsri et al. [28]. As such, the prepared fish scales were washed several times with distilled water to remove visible contaminants such as fat, sand, and salt and then dried at room temperature. The scales were then deproteinized for 5 hours with 0.1M hydrochloric acid. They were then washed with distilled water several times to neutralize. The remaining proteins in fish scales were then removed by washing with a 5% (w/v%) NaOH solution at 70 °C for 5 hours. The white precipitate was neutralized with distilled water and separated using centrifugation at 5000 rpm. The resulting white powder was dried at 60 °C and rinsed again for 1 hour at 100 °C at a concentration of 50% (w/v%). Following that, the prepared hydroxyapatite nanoparticles were washed and dried at a temperature of 60 °C.

Synthesis of magnetic iron oxide nanoparticles (Fe_3O_4)

Magnetic iron nanoparticles were synthesized using the chemical co-precipitation method [29]. Both $FeCl_3.6H_2O$ and $FeSO_4.7H_2O$ were dissolved in 100 ml of distilled water (the Fe(II)/Fe(III) molar ratio was 1:2) and stirred at 80 °C for 20 minutes. The solution was then rapidly added with 25% ammonium hydroxide. The solution's color changed to dark brown (pH>10) at this point.

After 30 minutes, the mixture was allowed to stand until the formation of nanoparticle crystals was complete, as described in the following equation.

$$FeSO_4.7H_2O + 2FeCl_3.6H_2O + 8NH_4OH \rightarrow Fe_3O_4 + 6NH_4Cl + (NH_4)_2SO_4 + 17H_2O \quad (7)$$

After several washes with distilled water to achieve a neutral pH, the magnetic nanoparticles were dried in an oven at 40 °C and stored for use in Fenton experiments.

Synthesis of magnetic hydroxyapatite nanoparticles

Magnetic hydroxyapatite nanoparticles were prepared using the co-precipitation method [29]. In 100 mL of water, 76.7 g of $FeCl_3.6H_2O$ and 4 g of $FeSO_4.7H_2O$ were dissolved and stirred in a 2:1 molar ratio. The solution was then supplemented with 1 g of the hydroxyapatite nanoparticles synthesized in the preceding step, and the pH was adjusted to 10 with NaOH. After 30 minutes of stirring, the mixture was centrifuged to separate the components (5000 rpm). Magnetized hydroxyapatite nanoparticles were washed with distilled water until their pH reached neutral and then dried for 24 hours at 40 °C.

Synthesis of sodium alginate nanocomposite catalysts

To prepare sodium alginate-magnetic hydroxyapatite nanocomposite (Alg-mHap), 2 g sodium alginate was mixed with distilled water (2 w/v%) for 7 hours. The alginate solution was then added 1 g of magnetic hydroxyapatite nanoparticles and thoroughly mixed and homogenized. The viscous solution obtained was added dropwise into a 0.5 M solution of $FeCl_3$ using a 1 mm diameter syringe. For 24 hours, the formed grains were immersed in an iron chloride solution. It was then rinsed several times with distilled water and left in distilled water for an additional 24 hours to remove any iron ions that did not react with the catalyst. Finally, the catalysts were stored in distilled water until further experiments could be conducted. Instead of magnetic hydroxyapatite nanoparticles, magnetic and hydroxyapatite nanoparticles were used to prepare Alg-Fe_3O_4 and Alg-Hap, respectively. Catalysts synthesized were kept in water and used wet in subsequent experiments.

Structural analysis of synthesized catalysts

In the wavelength range 400–4000 cm^{-1}, Fourier-Transform Infrared (FTIR) spectroscopy (Nicolet 560) was used to identify and determine the functional groups of the catalyst before the Fenton reaction and cefixime degradation. Before the heterogeneous Fenton process, the surface morphology of the catalysts was examined using field emission scanning electron microscopy (FESEM, Philips XL30, and Netherland). The amount of iron leached into the solution was determined using atomic absorption (AAS 8020, South Korea). The measurement of pore size and adsorption/desorption isotherms was analyzed using the Brunauer-Emmett-Teller (BET) theory to estimate the specific surface area (BELSORP MINI II, Microtrac Bel Corp, Japan). The magnetization behavior was measured by vibrating sample magnetometer (VSM), (LBKFB model, Meghnatis Kavir Kashan, Iran). X-ray diffraction technique was used, which provides detailed information about the crystal structure of chemical substances and compounds containing cobalt anode (Philips, X'Pert, Netherlands, and landa=1.54 $\AA$). The crystallite's size can be determined indirectly using X-ray diffraction. The Scherrer formula can be used for this purpose [28]:

$$D = \frac{k\ \lambda}{\beta Cos\Delta} \quad (8)$$

D denotes the size of the crystallite, k denotes the Scherer constant value of 0.9, β the actual diffraction line width (diffraction width at half the height of the most significant peak), and θ the desired diffraction angle.

Point of Zero Charge (pH_{pzc})

The point of zero charges (pH_{pzc}) was specified by using 0.01 M NaCl solution. First, the NaCl solutions' pH was set at 3-11 via adding an adequate value of 0.01 M and/or 0.1 M NaOH or HCl solution. Second, 0.1 g of catalyst was added into the solutions; then, the solutions' final pH was obtained after 48 h. The pH_{pzc} was obtained from the intersection point of the curve of pH_{final} vs. $pH_{initial}$.

Batch Fenton studies

To determine the effect of pH, a cefixime solution containing 20 mg/L was prepared and stabilized at the desired pH using HCl (3 M) and NaOH (1 M), followed by the addition of 3.6 g of the desired catalyst and stirring at 125 rpm in an incubator shaker. Cefixime concentration was determined using a spectrophotometer (Cary 50 bio UV-

visible, λ_{max} = 285 nm), and the calibration curve (R^2=99.98) and removal percentage of cefixime were calculated using the following equation:

$$\%R = \frac{C_0 - C_t}{C_0} \quad (9)$$

Where C_t (mg/L) is the cefixime concentration remaining after degradation at time t (min), and C_0 (mg/L) is the initial cefixime concentration. To determine the effect of catalyst amount, different amounts of catalyst (50, 72, and 90 gr/L) were added to a cefixime solution containing 20 mg/L cefixime at an optimal pH and 2 mM H_2O_2. Additionally, to determine the effect of the initial cefixime concentration, three samples (5, 20, and 30 mg/L) were prepared, the optimal pH was stabilized, 3.6 g of each catalyst was added, and the removal percentage was determined at various times.

To determine the effect of the initial concentration of hydrogen peroxide, four samples of cefixime solution (20 mg/L and optimal pH) and 3.6 g of each catalyst were prepared in various concentrations of hydrogen peroxide (1, 2, 3, and 10 mM), and the cefixime removal percentage was calculated using Equation 1. To determine the reusability of catalysts, they were rinsed several times with distilled water following one step of using the catalyst and performing the Fenton reaction under optimal conditions. Catalysts were reused under the same conditions as previously, and each catalyst was tested three times. Additionally, it should be noted that iron leaching was determined under optimal conditions.

Degradation kinetics

The zero-order kinetic equation is one of the kinetic equations examined during drug degradation. The concentration gradient with time is independent of the material concentration in this equation, implying that the drug degrades at a constant and linear rate.

$$C_t = k_0 t + C_0 \quad (10)$$

Furthermore, equations 11 and 12 employ first- and second-order kinetic equations, respectively [30]:

$$\ln\left(C_t / C_0\right) = k_1 t \quad (11)$$

$$\frac{1}{C_t} - \frac{1}{C_0} = k_2 t \quad (12)$$

Where k_0 (mg/L min), k_1 (1/min), and k_2 (L/mg min) are zero-order, first-order, and second-order reaction rate constants, respectively.

The Langmuir-Hinschelwood kinetic model can be used to express the speed of catalytic reactions such as heterogeneous Fenton. This model begins with the adsorption of the removal material on the catalyst's surface and continues with the chemical reaction occurring on the surface [31].

$$-\frac{dC}{dt} = \frac{k_{\deg} k_{ad} C}{1 + k_{ad}} \quad (13)$$

Where k_{ad} (L/mg) and K_{deg} (mg/L min) denote the rate constants for adsorption and surface reaction, respectively.

RESULTS AND DISCUSSION

FTIR analysis

Fig. 1 depicts the FTIR diagrams of Alg-Hap, Alg-mHap, and Alg-Fe_3O_4. For Alg-Hap, the phosphate group peak at 524.5 cm^{-1} corresponds to phosphate in the hydroxyapatite structure, the peak at 794-810 cm^{-1} corresponds to Na-O stretching vibrations, and the peak at 1041 cm^{-1} corresponds to C-O or C-O-C stretching vibrations that overlap with the C-O vibrations. The 1419 cm^{-1} wavelength is associated with the COO- asymmetric vibrations present in all three diagrams, whereas the 1620-1627 cm^{-1} wavelength is associated with the carboxylate group in the alginate structure. Additionally, the peak at approximately 3400 cm^{-1} is related to the hydroxyl group. The peak at 563.5 cm^{-1} in Alg-Fe_3O_4 was derived from the Fe-O bond in the synthetic composite structure. The phosphate group peak appears to overlap with the Fe-O stretching peak at 594 cm^{-1} for Alg-mHap. Interactions between functional groups can change the absorption strength, and or peak shape positioning. As can be seen in the spectrum of Alg-mHap, the peak intensities have decreased compared to the other two catalysts. Furthermore, peaks associated with the functional groups of the alginate polymer were observed in the composite spectrum. These interpretations imply that the catalyst used contains alginate, hydroxyapatite, and Fe_3O_4 nanoparticles [24,32–34].

Morphological analysis

Fig. 2 illustrates the surface morphology of the synthesized catalysts. Alg-Hap (Fig. 2a) has a nearly smooth surface with fine wrinkles. Alg-Fe_3O_4 (Fig.

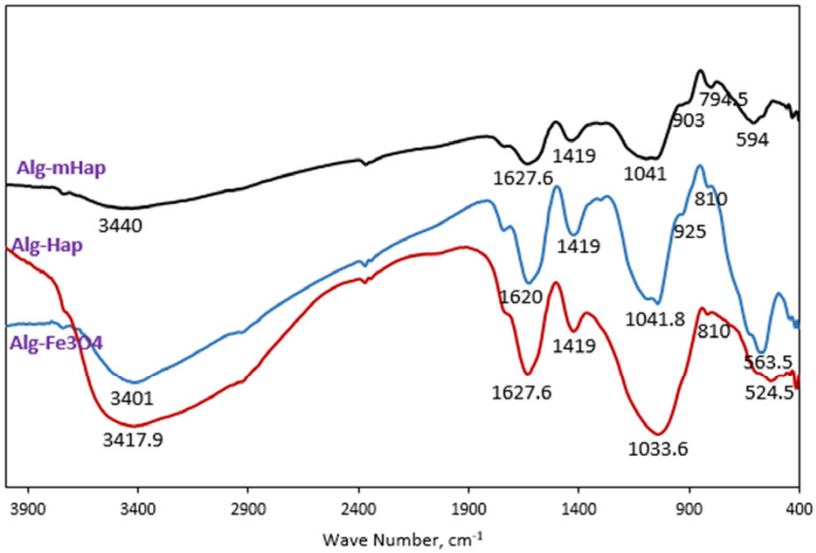

Fig. 1. FTIR analysis of Alg-Hap, Alg-Fe_3O_4 and Alg-mHap

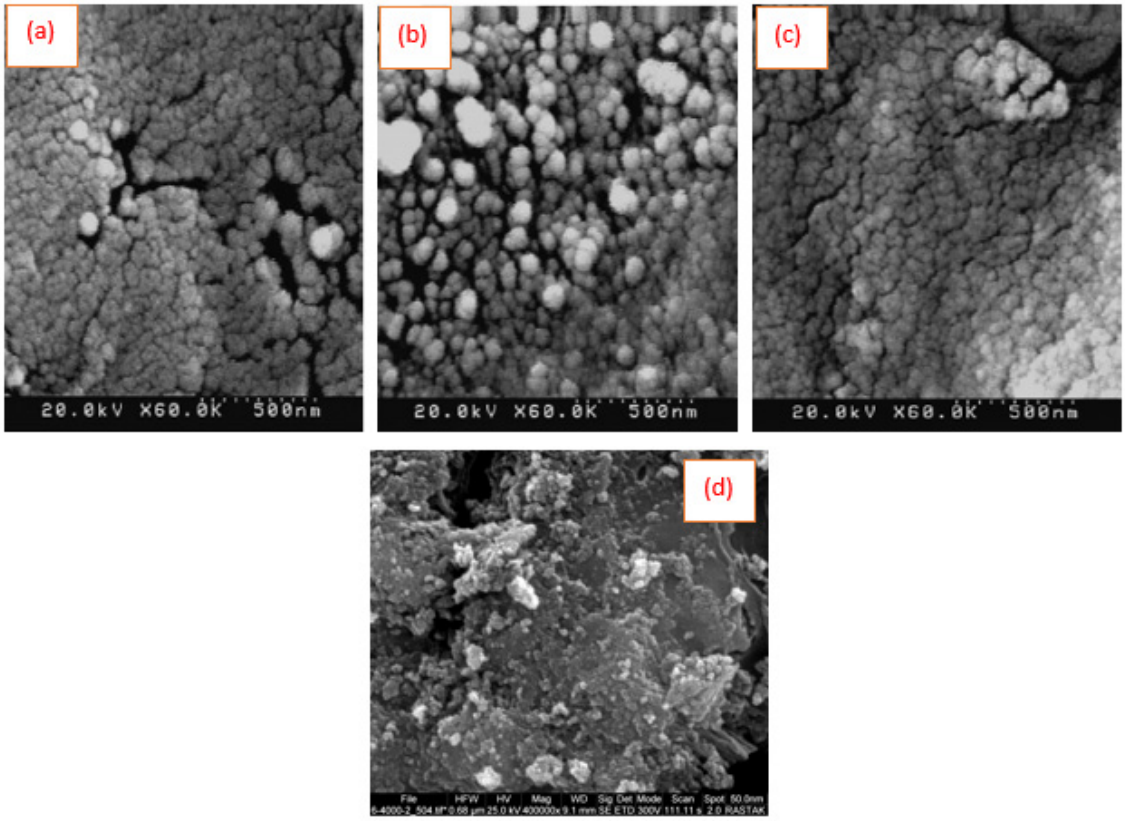

Fig. 2. SEM micrograph of (a) Alg-Hap (b) Alg-Fe_3O_4 (c) Alg-mHap (500 nm), and (d) Alg-mHap (50 nm)

2b) has a rough surface with an accumulation of magnetic NPs points. As shown in Fig. 2c and 2d, the surface of the Alg-mHap is wrinkled, but it also has large cracks due to the presence of magnetic hydroxyapatite nanoparticles. Meanwhile, it is clear that by adding Fe_3O_4 NPs and m-Hap, the surface of the catalysts reveals a rough morphology. By adding Fe_3O_4 and Hap NPs to the Alg network, the

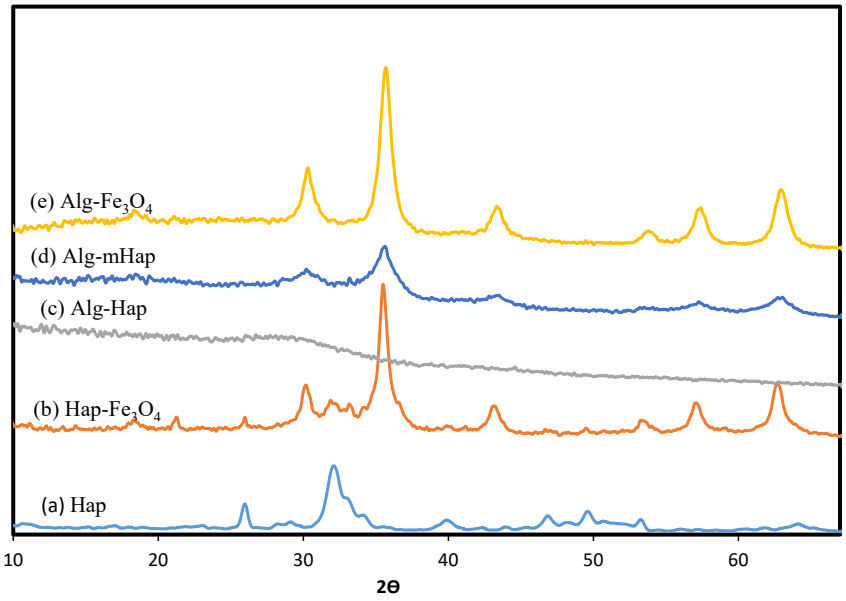

Fig. 3. X-ray diffraction of (a) Hap, (b) Hap-Fe_3O_4, (c) Alg-Hap, (d) Alg-mHap and (e) Alg-Fe_3O_4

Table 1. Information on crystal size and crystallinity percentage of synthesized samples

sample	crystallinity percentage	2θ (°)	D (nm)
Hap	55.83	32.3	6.9
Hap-Fe_3O_4	40.61	35.6	5.12
Alg-Hap	-	-	-
Alg-Fe_3O_4	28.47	35.8	7.59
Alg-mHap	13.6	35.7	4.38

surface was fully shielded with accumulated NPs, which were approximately spherical with formed aggregates. However, the presence of nanoparticles and agglomeration is clear, which can act as a place to adsorb cefixime.

X-ray diffraction analysis

Fig. 3 illustrates the results of X-ray diffraction analysis on the synthesized samples. Peaks observed in (2θ = 49.6, 46.9, 39.9, 2.33, 32, and 25.9°) hydroxyapatite (Fig. 3a) correspond well to the XRD pattern of hydroxyapatite found in the Joint Committee's diffraction standard card number [0033-24] and indicates the formation of the crystalline structure of hydroxyapatite [35]. Furthermore, in addition to hydroxyapatite diffraction, peaks at angles (2θ = 35.5, 62.8, 57, 43.3, 2.30, and 21.2°) were observed, which, according to JCPDS [0033-75], indicates the presence of Fe_3O_4 NPs in magnetic hydroxyapatite (Fig. 3b) [31,36]. The intensity of peaks decreased in the XRD pattern of the Alg-Hap catalyst (Fig. 3c), which could be due to the natural pattern of amorphous sodium alginate covering the surface of hydroxyapatite and overcoming its crystalline property or to the low amount of hydroxyapatite. Additionally, diffraction associated with magnetic nanoparticles is observed in the structure of Alg-Fe_3O_4 (Fig. 3d) and Alg-mHap (Fig. 3e) samples. However, in the Alg-mHap sample, no hydroxyapatite nanoparticle dispersions are observed in the catalyst structure, implying that this issue was caused by the amorphous structure of alginate and the relatively small amount of this nanoparticle in the catalyst structure.

Additionally, the percentage of crystallinity was determined by dividing the peaks' area by the XRD diagram's total area, as shown in Table 1. The results indicate that the presence of alginate polymer decreases the crystallinity percentage, whereas the presence of Fe_3O_4 NPs is critical for catalyst crystallization.

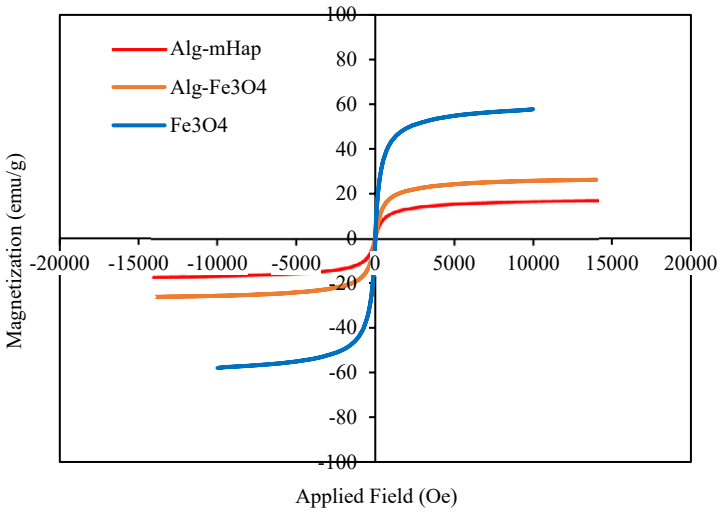

Fig. 4. Magnetic hysteresis loops of Fe_3O_4, Alg-Fe_3O_4, and Alg-mHap.

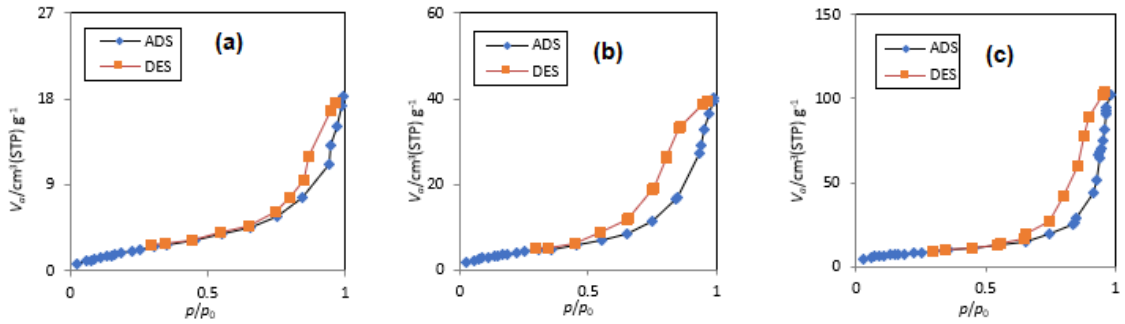

Fig. 5. N_2 adsorption-desorption isotherms for a) Alg-Hap, b) Alg-Fe_3O_4, and c) Alg-mHap.

VSM analysis

Fig. 4 shows the results of the VSM analysis of Fe_3O_4, Alg-Fe_3O_4, and Alg-mHap. A study of the curves revealed a decrease in the saturation magnetization value with 26 emu/g, and 16.6 emu/g for Alg-Fe_3O_4, and Alg-mHap, respectively, compared to Fe3O4 NPs (57.4 emu/g). This reduction of saturation magnetization is can be related to the size of particles, structure, morphology, and, the isolation effect of Alg and Hap [37]. It should be noted that almost no hysteresis loops were found in the magnetization curves, suggesting the superparamagnetic of Fe_3O_4, Alg-Fe_3O_4, and Alg-mHap. Furthermore, the Alg-Fe_3O_4 and Alg-mHap possess enough magnetization that gives them an advantage for practical application involving the dispersion of Alg-Fe_3O_4, and Alg-mHap catalysts in water and their collection using a magnetic field [38].

BET analysis

The specific surface area of Alg-Hap, Alg-Fe_3O_4, and Alg-mHap are found to be 7.92 m^2/g, 15.2 m^2/g, and 28.6 m^2/g, respectively. As a result, it can be established that the loading mHap into the Alg network has decreased the surface area of the catalyst and possessed effective adsorption properties. Adsorption/desorption diagrams obtained for all three catalysts are given in Fig. 5. The adsorption/desorption diagrams of the synthesized adsorbents are most similar to type IV of the IUPAC classification which confirmed the mesoporous characters of the obtained catalysts [39]. The total pore volume of Alg-mHap nanocomposites (0.157 cm^3/g) is higher than Alg-Fe_3O_4 (0.061 cm^3/g) and Alg-Hap (0.02 cm^3/g) which can increase its adsorption capacity. Therefore, the binding of mHap to the polymer chains can be lead to an increase in mesoporous at the Alg-mHap surface.

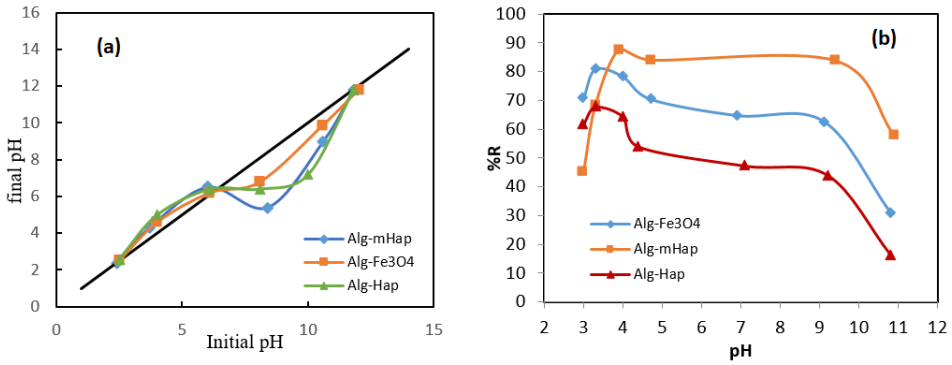

Fig. 6. a) pH of point zero charges of catalysts, b) Effect of initial pH on cefixime removal (H_2O_2 = 2 mM, catalyst amount =72 gr/L, cefixime concentartion = 20 mg/L)

Furthermore, the smaller surface area of Alg-Hap compared with Alg-Fe_3O_4 could be due to the aggregation of Hap nanoparticles.

Fenton process condition analysis

Effect of pH

An influential factor of pH-sensitive adsorbents is pH_{pzc}, which specifies the linearity of the pH sensitivity domain and then determines the surfaces' adsorption capabilities and the type of surface-active centers. At point zero charges (PZC) the total surface positive charge is in equilibrium with the overall negative charge of the surface. Also, the surface is charged positively below pH_{pzc}, while at pH values above pH_{pzc}, the surface is charged negatively [40]. The curves' intersection with the straight line for final pH vs initial pH gives the pH_{pzc} (Fig. 6a), and the amount is ~8.1 for all three catalysts.

Fig. 6b illustrates the effect of the initial pH of the solution on cefixime removal. According to the obtained data, Alg-Hap demonstrated the highest and lowest removal rates at pH 3.3 (67.7%) and pH 10.8 (16.37%), respectively. Alg-Fe_3O_4 also had the highest removal rate at pH 3.3 (80.9%) and the lowest removal rate at pH 10.8 (30.9%), while Alg-mHap had the highest and lowest removal rates at pH 4 and 10.8, respectively, of 87.7% and 57.7%. Alg-mHap's superior performance to the other two catalysts may be attributed to the deposition of magnetic nanoparticles on the hydroxyapatite substrate (as seen in SEM images). As a result, it can exert a greater degree of influence over the Fenton process.

On the other hand, hydroxyapatite is an excellent adsorbent for cefixime, which increases the catalyst's efficiency. The Fenton process's efficiency is highly dependent on the reaction medium's pH, and it is also more effective in an acidic environment than in an alkaline one [41]. At pH values less than 3.3, the free hydroxyl formed during the reaction of H_2O_2 and Fe^{2+} participates in reaction 14, lowering the cefixime removal percentage. Additionally, at pH values greater than 3.3 for Alg-Fe3O4 and Alg-Hap, and pH values greater than 4 for Alg-mHap, Fe^{3+} precipitated as $Fe(OH)_3$ and produced H_2O_2, which is unstable and decomposes into O_2 and H_2O, thereby losing its oxidizing properties [9,34].

$$OH^{\bullet} + H^{+} + e^{-} \rightarrow H_2O \qquad (14)$$

Effect of initial concentration of cefixime

Another critical aspect of the Fenton process to consider is the effect of the initial concentration of the material to be removed on its efficiency in real environments (Fig. 7). Alg-Hap's results indicated that increasing the initial cefixime concentration from 5 to 30 mg/L decreased the removal percentage from 70 to 60.5%. The removal percentage of Alg-Fe_3O_4 changed similarly at the same concentrations of 5, 20, and 30 mg/L, decreasing from 82.7 to 81 and 80.4%, respectively, and in the case of Alg-mHap, the removal percentage decreased from 88.7 to 84%, respectively, when the initial concentration of cefixime was increased from 5 to 30 mg/L. When high concentrations of cefixime are combined with a constant amount of H_2O_2 and catalyst, the generated free radicals are insufficient to remove all target pollutants. Additionally, the active sites of the radical reaction are limited. As a result, degradation is inhibited at high cefixime concentrations, necessitating additional time for drug degradation [42].

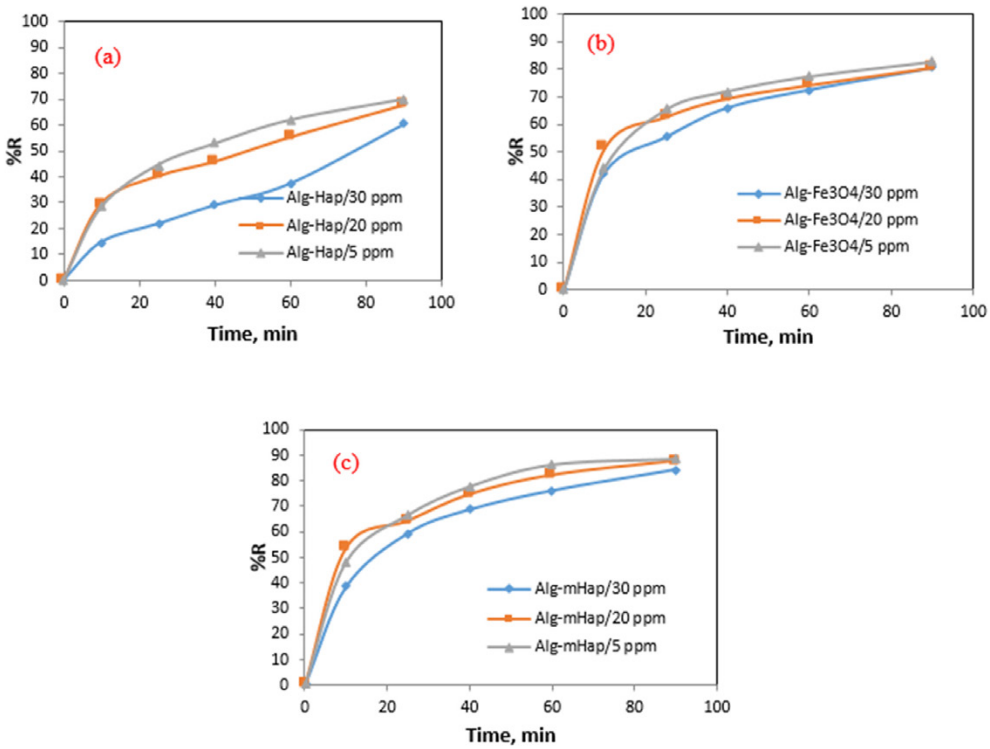

Fig. 7. Effect of initial cefixime concentration on cefixime removal (a) Alg-Hap, (b) Alg-Fe_3O_4 and (c) Alg-mHap (H_2O_2 = 2 mM, catalyst amount =72 gr/L, pH =4)

Effect of the catalyst amount

As illustrated in Fig. 8, increasing the amount of Alg-Hap catalyst from 50 to 90 gr/L increased the removal percentage from 64.8 to 71.2%, respectively, indicating that the removal percentage increases with increasing the amount of catalyst in other catalysts. By increasing the amount of Alg-Fe3O4 catalyst from 50 to 90 gr/L, the removal percentage increased from 80.7 to 83.9%, and by increasing the amount of Alg-mHap catalyst from 50 to 90 gr/L, the removal percentage increased from 86.7 to 91%. Although increasing the amount of catalyst had a negligible effect on the percentage of cefixime degradation, increasing the amount of catalyst also increases the number of active sites, effectively degrading hydrogen peroxide and producing more hydroxyl free radicals, which further degrades the cefixime [43].

Effect of hydrogen peroxide concentration

The concentration of hydrogen peroxide is critical in the Fenton reaction, which can have either positive or negative consequences. The results of the hydrogen peroxide concentration gradient are depicted in Fig. 9. According to the data, for all three catalysts, when the concentration of hydrogen peroxide was increased from 1 to 3 mM, the removal percentage increased approximately 8%. Given that the rate of cefixime degradation is proportional to the amount of hydroxyl radical produced, it is reasonable to assume that as the concentration of hydrogen peroxide increases, the percentage of antibiotics removed increases. However, increasing the concentration of hydrogen peroxide to 10 mM had no effect, and even the removal percentage decreased. Furthermore, the same holds for the other two catalysts, with the removal percentage in Alg-Fe_3O_4 decreasing from 83.3 to 76.9% when the hydrogen peroxide concentration was increased from 3 to 10 mM, and in Alg-mHap decreasing from 90 to 82.2% when the hydrogen peroxide concentration was increased from 3 to 10 mM. This decrease in removal percentage could be due to one of two factors. Initially, alginate inhibits hydroxyl production and competes with cefixime during the degradation process by increasing the concentration of hydrogen peroxide and producing excess free radicals [24,42]. This is naturally possible when the catalyst beads degrade, and iron ions diffuse into the aqueous medium on the surface,

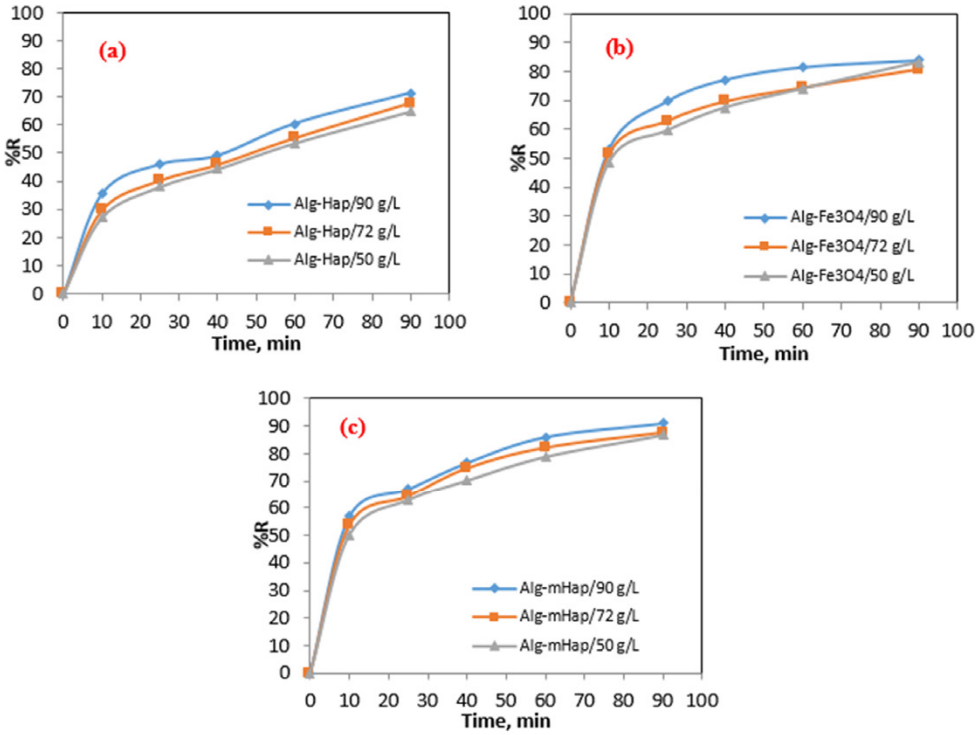

Fig. 8. Effect of catalyst amount on cefixime removal (a) Alg-Hap, (b) Alg-Fe_3O_4 and (c) Alg-mHap (H_2O_2=2 mM, cefixime concentration=20 mg/L, pH =4)

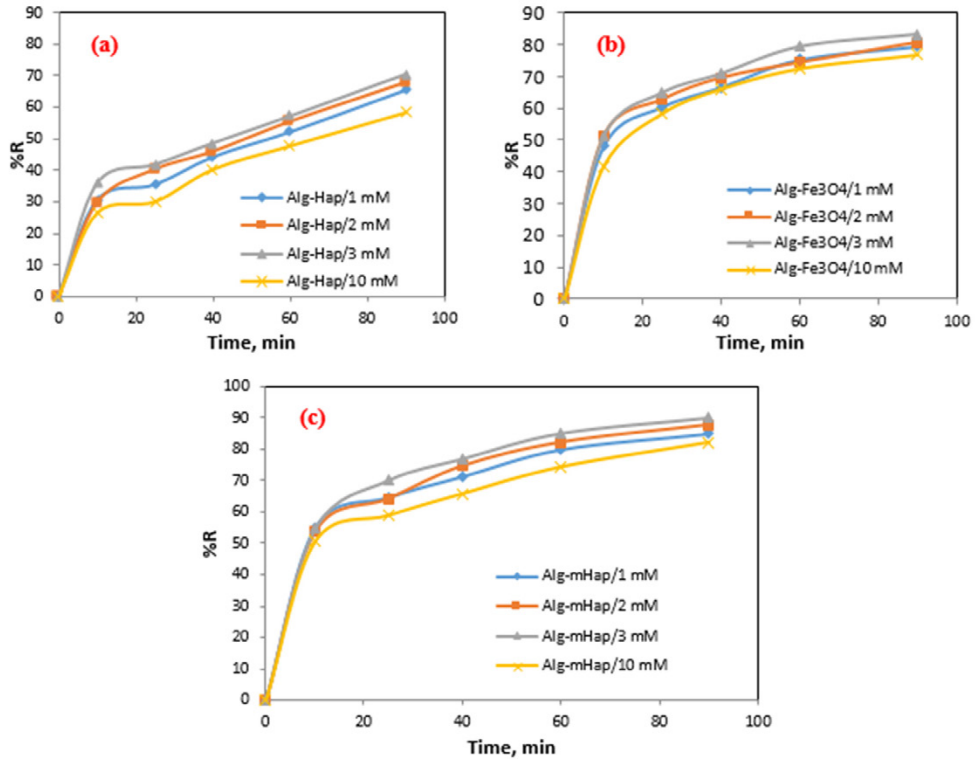

Fig. 9. Effect of hydrogen peroxide concentration on cefixime removal (a) Alg-Hap, (b) Alg-Fe_3O_4 and (c) Alg-mHap (catalyst amount = 72 g/L, cefixime concentration=20 mg/L, pH =4)

as demonstrated in the following section (release of iron ions). Second, H_2O_2 is a potent hydroxyl scavenger at high concentrations (reactions 15 and 16). Excessive hydrogen peroxide concentrations result in the formation of less active hydroperoxy radicals that are significantly less reactive with organic molecules [44]. As a result, it is possible to conclude that cefixime degrades rapidly at low H_2O_2 concentrations.

$$H_2O_2 + OH^{\cdot} \rightarrow H_2O + OOH^{\cdot} \quad (15)$$

$$OOH^{\cdot} + OH^{\cdot} \rightarrow H_2O + O_2 \quad (16)$$

Evaluation of iron leaching from the catalyst beads

The highest amount of iron released was 8.89 mg/L from the Alg-Fe_3O_4 catalyst. After the Fenton process, the concentration of iron ions was measured to be 2.6 mg/L in a solution containing the Alg-Hap catalyst and 0.92 mg/L in a solution containing the Alg-mHap catalyst. According to the results and Iranian water standards, a concentration of 0.3 to 2 mg/L is considered safe for drinking, while a 5 to 20 mg/L concentration is considered safe for agricultural use. Additionally, concentrations less than 1 mg/L are suitable for industrial use, depending on the type of industrial activity. As a result, the amount of iron released by all synthesized catalysts is within an acceptable range.

Reusability and oxidative behavior of the synthesized catalyst beads

Reusability of the catalyst is one of the most critical considerations when working with a heterogeneous catalyst. Catalyst beads must be reusable to be used on a large scale. Consecutive experiments with the same recovered beads were conducted following each stage of their application in this regard. After three times, the Alg-mHap catalyst's removal percentage decreased from 87.67 to 77.95 and 77.14%, respectively. After three catalyst use and recovery stages, the Alg-Fe_3O_4 catalyst's removal percentage decreased from 80.91 to 76.47 and 72.69%, respectively. In the case of the Alg-Hap catalyst, the removal percentage did not decrease significantly after three stages of use (80 to 69.7%), which is an excellent result for a heterogeneous Fenton process catalyst.

Alg-mHap has the highest removal percentage of all other catalysts (91%), as illustrated in Fig. 10a. The Fenton reaction with Alg-Fe_3O_4 and Alg-Hap is followed by the Fenton reaction with Alg-Fe_3O_4 and Alg-Hap at 84 and 71.2%, respectively. Without adding hydrogen peroxide (adsorption), the Alg-mHap, Alg-Fe_3O_4, and Alg-Hap catalysts removed 48.6%, 30.7%, and 25.8% of cefixime, respectively, indicating that the Alg-mHap catalyst is a better adsorbent for cefixime than the other two catalysts.

The degradation of cefixime on the surface of an Alg-mHap catalyst in the presence of H_2O_2 is depicted schematically (Fig. 10b). The catalyst's surface is highly pH-dependent due to the presence of carboxylate functional groups in alginate and phosphate functional groups in hydroxyapatite. At pH=3, the non-ionized functional groups of cefixime and the catalyst ($COOH$ and H_3PO_4) reduce electrostatic repulsion between the catalyst and cefixime. As a result, the cefixime is readily adsorbed to the catalyst surface via hydrogen bonding.

Due to the presence of Fe^{2+} and Fe^{3+} in MNPs and Fe^{3+} as a crosslinker of polymer chains, the Fe^{3+}/Fe^{2+} redox cycle is initiated in the Alg-mHAp catalyst via reactions 1-3. This process is analogous to that which occurs in a homogeneous Fenton system.

Additionally, mHAp provides additional active sites for H_2O_2 adsorption on the catalyst surface. Furthermore, adding HAp and mHAp increases the catalyst's active sites, increasing the mass transfer of organic pollutants between the liquid phase and the catalyst surface. Eventually, cefixime molecules are attacked and converted to CO_2 and H_2O by $OH^{\cdot}$ radicals formed on the surface of Alg-mHAp catalysts.

Degradation kinetics and mechanism

Table 2 summarizes the effect of various parameters on the kinetic constants and R^2 values. The study results on the degradation kinetics of all three catalysts using zero, first, and second-order kinetic models demonstrated that the experimental data fit well with the second-order degradation kinetics equation. According to the obtained results, the constant rate of degradation decreases as the concentration of cefixime increases, and it can also be stated that the Alg-mHap catalyst is more efficient than the other two catalysts at a constant cefixime concentration. Furthermore, increasing the concentration of hydrogen peroxide from 1 to 3 mM increased the rate constant from 0.0023 to 0.0059, while increasing the hydrogen peroxide concentration to 10 mM decreased it to

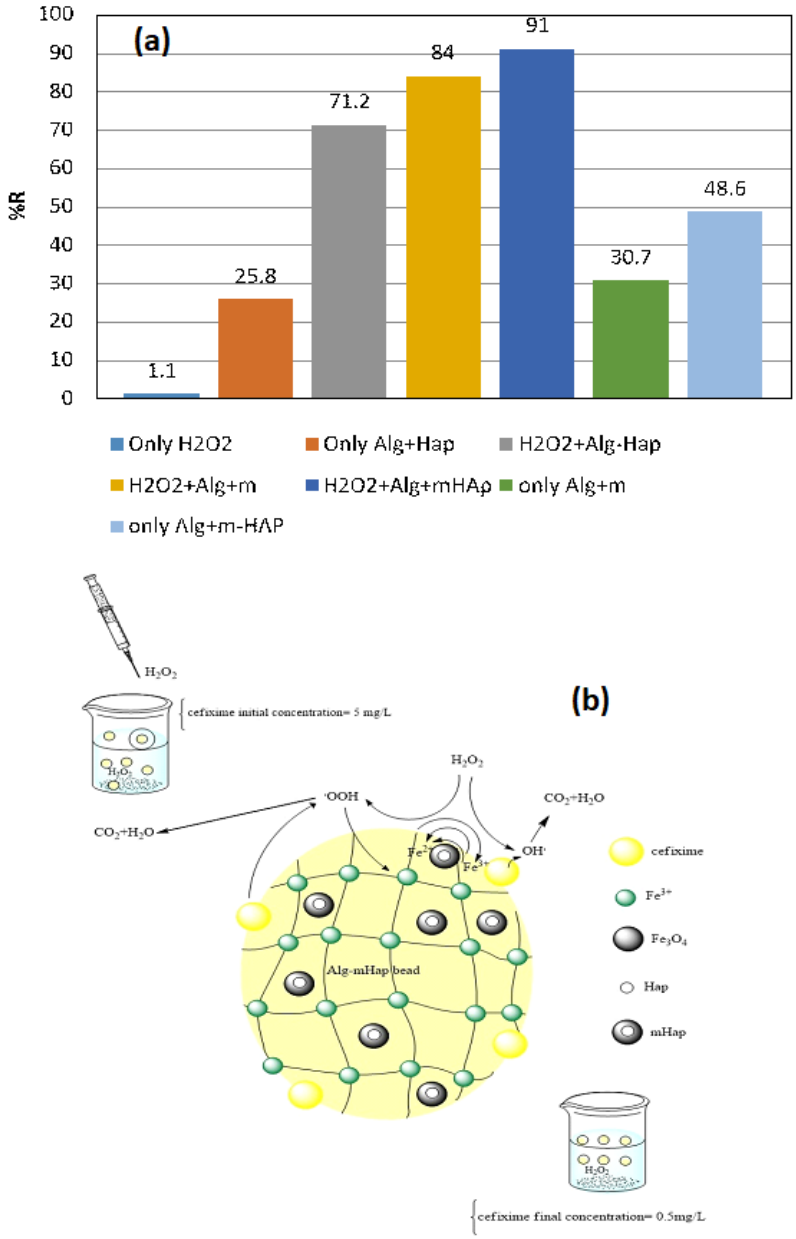

Fig. 10. (a) Comparison of different methods for removal cefixime removal (in optimal conditions) (b) The schematic of the proposed cefixime degradation by Alg-mHAp catalyst in the Fenton process.

0.0019. The results indicate that Alg-mHap has a greater removal rate than the other two catalysts. By increasing the Alg-Fe_3O_4 amount from 50 to 90 gr/L, the degradation reaction rate constant was increased from 0.0014 to 0.0024, while, for the Alg-mHap catalyst was increased from 0.0021 to 0.0038, and for the Alg-Hap catalyst was increased from 0.0008 to 0.0013. Table 3 also includes the results of the Langmuir-Hinschelwood equation constant. As can be seen, the degradation reaction rate constant was significantly more significant than the adsorption reaction rate constant, indicating that the cefixime degradation process had a more significant effect on the adsorption reaction during the Fenton process.

A comparison between the results of this study and other similar studies using the AOP process to degradation of cefixime from an aqueous solution

Table 2. Kinetic constants during the Fenton process

	Catalyst	H_2O_2 concentration (mM)	R^2	k_0 (mg/L min)	Concentration of cefixime (mg/L)	R^2	k_0 (mg/L min)	Catalyst dosage (g/L)	R^2	k_0 (mg/L min)
Zero Order	Alg-mHap	1	0.7092	0.0153	5	0.7259	0.0398	50	0.7607	0.1575
		2	0.727	0.1682	20	0.727	0.1628	72	0.728	0.1628
		3	0.6447	0.1666	30	0.751	0.2352	90	0.6672	0.1545
		10	0.7369	0.1487						
	Alg-Fe_3O_4	1	0.7048	0.1369	5	0.762	0.0442	50	0.7315	0.1409
		2	0.6888	0.1449	20	0.6888	0.1449	72	0.6888	0.1449
		3	0.6452	0.1491	30	0.7629	0.2142	90	0.6787	0.1591
		10	0.7345	0.1366						
	Alg-Hap	1	0.8928	0.134	5	0.798	0.0311	50	0.8778	0.1263
		2	0.8527	0.1177	20	0.8557	0.1177	72	0.8557	0.1177
		3	0.8456	0.1471	30	0.9766	0.1789	90	0.8441	0.1409
		10	0.9198	0.1148						
	Catalyst	H_2O_2 concentration (mM)	R^2	k_1 (1/min)	Concentration of cefixime (mg/L)	R^2	k_1 (1/min)	Catalyst dosage (gr/L)	R^2	k_1 (1/min)
First Order	Alg-mHap	1	0.9009	0.0172	5	0.965	0.0259	50	0.9217	0.0167
		2	0.9175	0.0194	20	0.9175	0.0194	72	0.9175	0.0194
		3	0.9236	0.0255	30	0.9259	0.0174	90	0.8944	0.0211
		10	0.9128	0.0155						
	Alg-Fe_3O_4	1	0.8528	0.0138	5	0.9672	0.0274	50	0.8782	0.0133
		2	0.8572	0.0151	20	0.8572	0.0151	72	0.8572	0.0151
		3	0.8574	0.0174	30	0.8896	0.0133	90	0.8822	0.0175
		10	0.8598	0.0124						
	Alg-Hap	1	0.9659	0.01	5	0.9258	0.0122	50	0.9587	0.01
		2	0.9513	0.0108	20	0.9513	0.0108	72	0.9513	0.0108
		3	0.9555	0.0126	30	0.9813	0.0088	90	0.9567	0.0127
		10	0.9742	0.0085						
	Catalyst	H_2O_2 concentration (mM)	R^2	k_2 (L/mg min)	Concentration of cefixime (mg/L)	R^2	k_2 (L/mg min)	Catalyst dosage (g/L)	R^2	k_2 (L/mg min)
Second Order	Alg-mHap	1	0.9941	0.0023	5	0.9553	0.0252	50	0.9971	0.0021
		2	0.9992	0.0029	20	0.9992	0.0029	72	0.9992	0.0029
		3	0.9836	0.0059	30	0.9979	0.0016	90	0.9983	0.0038
		10	0.9922	0.0019						
	Alg-Fe_3O_4	1	0.9604	0.0016	5	0.9752	0.0267	50	0.9748	0.0014
		2	0.972	0.0019	20	0.972	0.0019	72	0.972	0.0019
		3	0.9805	0.0025	30	0.9742	0.0009	90	0.9919	0.0024
		10	0.9509	0.0012						
	Alg-Hap	1	0.982	0.0008	5	0.9902	0.0053	50	0.9855	0.0008
		2	0.9792	0.0011	20	0.9792	0.0011	72	0.9792	0.0011
		3	0.9696	0.0012	30	0.9516	0.0005	90	0.9856	0.0013
		10	0.9949	0.0007						

Table 3. Langmuir-Hinschelwood kinetic constants

Catalyst	Adsorption reaction rate constant	Degradation reaction rate constant	R^2
Alg-mHap	0.0216	1.298	0.9698
Alg-Fe_3O_4	0.0522	0.632	0.966
Alg-Hap	0.0166	0.8187	0.8489

Table 4. Comparison of the cefixime removal percentage in different studies

Reference	Method	Catalyst	Removal (%)
This study	Heterogenous Fenton	Alg-mHap	91
This study	Heterogenous Fenton	Alg-Fe_3O_4	84
This study	Heterogenous Fenton	Alg-Hap	71.2
[2]	UV/H_2O_2 process	-	100
[6]	Photo-catalyst	$BiFeO_3$/Magnetic nanocomposite	91.8
[8]	Photo-catalyst	α-Fe_2O_3/ZnO	80
[1]	Sono-electro-Fenton	-	97.5
[45]	Photo-catalyst	MIL-53(Fe)/urchin-like g-C3N4 nanocomposite	94%
[46]	Photocatalytic (visible light)-ozonation	Nano N-TiO2/graphene oxide/titan grid sheets	80%
[47]	Photo-catalyst (UV/A)	TiO2/GO/chitosan	95.34%
[48]	Photo-catalyst (UV/A)	SWCNT/ZnO/Fe3O4	94.19

is shown in Table 4. According to the operating conditions used in each study, it is observed that the removal percentage of cefixime in the present study is equal to or higher than other studies. This can be related to the different conditions used in each experiment.

CONCLUSIONS

Three polymeric catalysts were synthesized in this study using alginate polymer, magnetite nanoparticles, and magnetic hydroxyapatite nanoparticles and were used to remove cefixime in a heterogeneous Fenton process. FTIR analysis confirmed the presence of functional groups in the structure of the synthesized catalyst beads, whereas SEM, VSM, and XRD analysis confirmed the presence of hydroxyapatite and Fe_3O_4 nanoparticles in the structure of the catalysts. The optimal pH was 3.3 for Alg-Fe_3O_4 and Alg-Hap and 4 for Alg-mHap. The results indicated that as the initial concentration of cefixime and the amount of catalyst increase, the percentage of cefixime removed decreases and increases, respectively. Calculating the degradation reaction rate and the adsorption reaction constants revealed that the degradation reaction occurs more rapidly than the adsorption reaction over the surface of all three catalysts. When the efficiency of the catalysts in the heterogeneous Fenton process was compared, it was determined that Alg-mHap performed better than the other two catalysts. Moreover, the Alg-mHap catalyst releases fewer iron ions than the other two catalysts. When kinetic equations were used to analyze the experimental results, it became clear that the data were more consistent with the second kinetic equation.

CONFLICT OF INTEREST

The authors declare that they have no known competing financial interests or personal relationships that could have appeared to influence the work reported in this paper.

REFERENCES

1. Hasani K, Peyghami A, Moharrami A, Vosoughi M. 2020 The efficacy of sono-electro-Fenton process for removal of Cefixime antibiotic from aqueous solutions by response surface methodology (RSM) and evaluation of toxicity of effluent by microorganisms. Arabian Journal of Chemistry, 13(7), 6122–6139. doi:10.1016/j.arabjc.2020.05.012.
2. Belghadr I, Shams Khorramabadi G, Godini H, Almasian M. 2014 The removal of the cefixime antibiotic from aqueous solution using an advanced oxidation process (UV/H_2O_2). Desalination and Water Treatment, 55(4), 1068–1075. doi:10.1080/19443994.2014.928799
3. Cruz A, Couto L, Esplugas S, Sans C. 2016 Study of the contribution of homogeneous catalysis on heterogeneous Fe(III)/alginate mediated photo-Fenton process. Chemical Engineering Journal, 318, 272–280. http://dx.doi.org/10.1016/j.cej.2016.09.014.
4. El-ghenymy A, Rodríguez RM, Brillas E, Oturan N, Oturan MA. 2014 Electro-Fenton degradation of the antibiotic sulfanilamide with Pt/carbon-felt and BDD/carbon-felt cells. Kinetics, reaction intermediates, and toxicity assessment. Environmental Science and Pollution Research, 21, 8368–8378. doi:10.1007/s11356-014-2773-3
5. Hapeshi E, Achilleos A, Vasquez MI, Michael C, Xekoukoulotakis NP, Mantzavinos D, Kassinos D. 2010 Drugs degrading photocatalytically : Kinetics and mechanisms of ofloxacin and atenolol removal on titania suspensions. Water Research, 44(6), 1737–1746. http://dx.doi.org/10.1016/j.watres.2009.11.044.
6. Mostafaloo R, Mahmoudian MH, Asadi-ghalhari M. 2019 $BiFeO_3$/Magnetic nanocomposites for the photocatalytic degradation of cefixime from aqueous solutions under visible light. Journal of

Photochemistry & Photobiology, A: Chemistry, 382, 111926. doi:10.1016/j.jphotochem.2019.111926.
7. Rasoulifard MH, Khanmohammadi S, Heidari A. 2016 Adsorption of cefixime from aqueous solutions using modi fi ed hardened paste of Portland cement by perlite ; optimization by Taguchi method. Water Science and Technology, 75(4), 1069–1078. doi:10.2166/wst.2016.230
8. Shooshtari NM. Ghazi MM. 2017 An investigation of the photocatalytic activity of nano α-Fe_2O_3/ZnO on the photodegradation of cefixime trihydrate. Chemical Engineering Journal, 315, 527–536. http://dx.doi.org/10.1016/j.cej.2017.01.058.
9. Wang N, Zheng T, Zhang G, Wang P. 2016 A review on Fenton-like processes for organic wastewater treatment. Journal of Environmental Chemical Engineering, 4, 762–787. http://dx.doi.org/10.1016/j.jece.2015.12.016.
10. Lu Z, Ma Y, Zhang J, Fan N, Huang B, Jin R. 2020 A critical review of antibiotic removal strategies : Performance and mechanisms. Journal of Water Process Engineering, 38, 101681. doi:10.1016/j.jwpe.2020.101681.
11. Lima VB, Goulart LA, Rocha RS, Steter JR, Lanza MRV. 2020 Degradation of antibiotic ciprofloxacin by different AOP systems using electrochemically generated hydrogen peroxide. Chemosphere, 247, 125807. doi:10.1016/j.chemosphere.2019.125807.
12. Molina CB, Sanz-Santos E, Boukhemkhem A, Bedia J, Belver C, Rodriguez JJ. 2020 Removal of emerging pollutants in aqueous phase by heterogeneous Fenton and photo-Fenton with Fe_2O_3-TiO_2-clay heterostructures. Environmental Science and Pollution Research, 27, 38434–38445. doi:10.1007/s11356-020-09236-8
13. Huang M, Zhou T, Wu X, Mao J. 2015 Adsorption and degradation of norfloxacin by a novel molecular imprinting magnetic Fenton-like catalyst. Chinese Journal of Chemical Engineering, 23(10), 1698–1704. http://dx.doi.org/10.1016/j.cjche.2015.08.030.
14. Pukdee-asa M. Su C. 2011 Degradation of azo dye by the fluidised-bed Fenton process. Coloration Technology, 128(1), 28–35. doi:10.1111/j.1478-4408.2011.00325.x
15. Nazari P, Askari N, Setayesh SR. 2020 Oxidation-precipitation of magnetic Fe_3O_4/AC nanocomposite as a heterogeneous catalyst for electro-Fenton treatment. Chemical Engineering Communications, 207(5), 1–11. doi:10.1080/00986445.2019.1613233.
16. Benincá C, Boni EC, Gonçalves FF, Primel G, Freire FB, Zanoelo EF. 2018 Photo-fenton and UV photo degradation of naphthalene with zero- and two-valent iron in the presence of persulfate two-valent iron in the presence of persulfate. Chemical Engineering Communications, 206(1), 1–11. doi:10.1080/00986445.2018.1469015.
17. Homem V, Santos L. 2011 Degradation and removal methods of antibiotics from aqueous matrices e A review. Journal of Environmental Management, 92(10), 2304–2347. http://dx.doi.org/10.1016/j.jenvman.2011.05.023.
18. Wang L, Lei J, Liu Y, Zhang J. 2016 Well dispersed Fe2O3 nanoparticles on g-C_3N_4 for efficient and stable photo-Fenton photocatalysis under visible light irradiation. European Journal of Inorganic Chemistry, 2016(34), 5387–5392. doi:10.1002/ejic.201600959
19. Luo M, Bowden D, Brimblecombe P. 2009 Catalytic property of Fe-Al pillared clay for Fenton oxidation of phenol by H_2O_2. Applied Catalysis B: Environmental, 85, 201–206. doi:10.1016/j.apcatb.2008.07.013
20. Liu Y, Zhong H, Li L, Zhang C. 2010 Temperature dependence of magnetic property and photocatalytic activity of Fe_3O_4/hydroxyapatite nanoparticles. Materials Research Bulletin, 45(12), 2036–2039. http://dx.doi.org/10.1016/j.materresbull.2010.09.010.
21. Xu P, Ming G, Lian D, Ling C, Hu S, Hua M. 2012 Use of iron oxide nanomaterials in wastewater treatment : A review. Science of the Total Environment, The, 424, 1–10. http://dx.doi.org/10.1016/j.scitotenv.2012.02.023.
22. Chatzimarkou A, Stalikas C. 2020 Adsorptive removal of estriol from water using graphene-based materials and their magnetite composites: heterogeneous fenton-like non-toxic degradation on magnetite/graphene oxide. International Journal of Environmental Research, 74(5), 1069–1078. doi:10.1007/s41742-020-00255-4.
23. Luo Y, Lode A, Wu C, Chang J, Gelinsky M. 2015 Alginate/nanohydroxyapatite scaffolds with designed core/shell structures fabricated by 3d plotting and in situ mineralization for bone tissue engineering. ACS applied materials & interfaces, 7(12), 6541–6549. doi:10.1021/am508469h
24. Quadrado RFN, Fajardo AR. 2017 Fast decolorization of azo methyl orange via heterogeneous Fenton and Fenton-like reactions using alginate-Fe^{2+}/Fe^{3+}. Carbohydrate Polymers, 177, 443–450. http://dx.doi.org/10.1016/j.carbpol.2017.08.083.
25. Li Y, Wang S, Zhang Y, Han R, Wei W. 2017 Enhanced tetracycline adsorption onto hydroxyapatite by Fe(III) incorporation. Journal of Molecular Liquids, 247, 171–181. doi:10.1016/j.molliq.2017.09.110.
26. Pai S, Kini SM, Selvaraj R, Pugazhendhi A. 2020 A review on the synthesis of hydroxyapatite , its composites and adsorptive removal of pollutants from wastewater. Journal of Water Process Engineering, 38, 101574. doi:10.1016/j.jwpe.2020.101574.
27. Ergüt M, Uzunoğlu D, Özer A. 2019 Efficient decolourization of malachite green with biosynthesized iron oxide nanoparticles loaded carbonated hydroxyapatite as a reusable heterogeneous Fenton-like catalyst. Journal of Environmental Science and Health, Part A, 54(8), 1–15. doi:10.1080/10934529.2019.1596698.
28. Kongsri S, Janpradit K, Buapa K, Techawongstien S, Chanthai S. 2013 Nanocrystalline hydroxyapatite from fish scale waste: Preparation, characterization and application for selenium adsorption in aqueous solution. Chemical Engineering Journal, 215–216, 522–532. http://dx.doi.org/10.1016/j.cej.2012.11.054.
29. Ahmadifar Z, Dadvand Koohi A. 2018 Characterization, preparation, and uses of

nanomagnetic Fe_3O_4 impregnated onto fish scale as more efficient adsorbent for Cu^{2+} ion adsorption. Environmental Science and Pollution Research, 25(20), 19687–19700. doi:10.1007/s11356-018-2058-3
30. Nitoi I, Oncescu T, Oancea P. 2013 Mechanism and kinetic study for the degradation of lindane by photo-Fenton process. Journal of Industrial and Engineering Chemistry, 19(1), 305–309. http://dx.doi.org/10.1016/j.jiec.2012.08.016.
31. Valizadeh S, Rasoulifard MH, Seyed Dorraji MS. 2014 Modified Fe_3O_4-hydroxyapatite nanocomposites as heterogeneous catalysts in three UV, Vis and Fenton like degradation systems. Applied Surface Science, 319, 358–366. http://dx.doi.org/10.1016/j.apsusc.2014.07.139.
32. Abou Taleb MF, Alkahtani A, Mohamed SK. 2015 Radiation synthesis and characterization of sodium alginate/chitosan/hydroxyapatite nanocomposite hydrogels: a drug delivery system for liver cancer. Polymer Bulletin, 72, 725–742. doi:10.1007/s00289-015-1301-z
33. Thakur S, Pandey S, Arotiba OA. 2016 Development of a sodium alginate-based organic/inorganic superabsorbent composite hydrogel for adsorption of methylene blue. Carbohydrate Polymers, 153, 34–46. http://dx.doi.org/10.1016/j.carbpol.2016.06.104.
34. Dinarvand M, Sohrabi M, Royaee SJ, Zeynali V. 2017 Degradation of phenol by heterogeneous Fenton process in an impinging streams reactor with catalyst bed. Asia-Pacific Journal Of Chemical Engineering, 12(4), 2–10. doi:10.1002/apj.2104
35. Sundaram CS, Viswanathan N, Meenakshi S. 2008 Defluoridation chemistry of synthetic hydroxyapatite at nano scale : Equilibrium and kinetic studies. Journal of Hazardous Materials, 155, 206–215. doi:10.1016/j.jhazmat.2007.11.048
36. Minella M, Marchetti G, Laurentiis E De, Malandrino M, Maurino V, Minero C, Vione D, Hanna K. 2014 Photo-Fenton oxidation of phenol with magnetite as iron source. Applied Catalysis B, Environmental, 154–155, 102–109. http://dx.doi.org/10.1016/j.apcatb.2014.02.006.
37. Kara GK, Rabbani M. 2019 Experimental Study of Methylene Blue Adsorption from Aqueous Solutions onto Fe3O4/NiO Nano Mixed Oxides Prepared by Ultrasonic Assisted Co-precipitation, J. Nanostructures. 9, 287–300. doi:10.22052/JNS.2019.02.011.
38. Gemeay A, Keshta BE, El-sharkawy RG, Zaki A. 2020 Chemical insight into the adsorption of reactive wool dyes onto amine- functionalized magnetite/silica core-shell from industrial wastewaters, Environ. Sci. Pollut. Res. 27, 32341–32358. doi:10.1007/s11356-019-06530-y.
39. Rahmani M, Dadvand Koohi A, Faculty, 2021 Adsorption of malachite green on the modified montmorillonite / Xanthan xanthan gum-sodium alginate hybrid nanocomposite, Polym. Bull. in press.
40. Gholami Ahmadgurabi N, Dadvand Koohi A, Ebrahimian Pirbazari A. 2018 Fabrication , Characterization , Regeneration and Application of Nanomagnetic Fe3O4@Fish Scale as a Bio-adsorbent for Removal of Methylene Blue, J. Water Environ. Nanotechnol. 3, 219–234. doi:10.22090/jwent.2018.03.003.
41. Bai J, Liu Y, Yin X, Duan H, Ma J. 2017 Efficient removal of nitrobenzene by Fenton-like process with Co-Fe layered double hydroxide. Applied Surface Science, 416, 45–50. http://dx.doi.org/10.1016/j.apsusc.2017.04.117.
42. Kong Y, Zhuang Y, Shi B. 2019 Tetracycline removal by double-metal-crosslinked alginate/ graphene hydrogels through an enhanced Fenton reaction. Journal of Hazardous Materials, 382, 121060. doi:10.1016/j.jhazmat.2019.121060.
43. Wang X, Zhuang Y, Zhang J, Song L, Shi B. 2020 Degradation behaviors in a heterogeneous Fenton system through Fe/S-doped aerogel. Science of the Total Environment, 714, 136436. doi:10.1016/j.scitotenv.2019.136436.
44. Hammouda SB, Adhoum N, Monser L. 2015 Synthesis of magnetic alginate beads based on Fe_3O_4 nanoparticles for the removal of 3-methylindole from aqueous solution using Fenton process. Journal of Hazardous Materials, 294, 128–136. http://dx.doi.org/10.1016/j.jhazmat.2015.03.068.
45. Salimi M, Esrafili A, Jafari AJ, Gholami M, Sobhi HR. 2019 Application of MIL-53(Fe)/urchin-like g-C3N4 nanocomposite for efficient degradation of cefixime, Inorg. Chem. Commun. 53, 107565. doi:10.1016/j.inoche.2019.107565.
46. Sheydaei M, Reza H, Shiadeh K, Ayoubi-feiz B, Ezzati R. 2018 Preparation of nano N-TiO 2 / graphene oxide / titan grid sheets for visible light assisted photocatalytic ozonation of ce fi xime, Chem. Eng. J. 353, 138–146. doi:10.1016/j.cej.2018.07.089.
47. Erim B, Ciğeroğlu Z, Bayramoğlu M. 2021 Green synthesis of TiO2/GO/chitosan by using leaf extract of Olea europaea as a highly efficient photocatalyst for the degradation of cefixime trihydrate under UV-A radiation exposure : An optimization study with d-optimal design, J. Mol. Struct. 1234, 130194. doi:10.1016/j.molstruc.2021.130194.
48. Erim B, Ciğeroğlu Z, Şahin S, Vasseghian Y. 2022 Photocatalytic degradation of cefixime in aqueous solutions using functionalized SWCNT/ZnO/Fe3O4 under UV-A irradiation, 291(2), 132929. doi:10.1016/j.chemosphere.2021.132929